

# 1 Surface deposition of marine fog and its treatment in the WRF 2 model

3 Peter A. Taylor<sup>1</sup>, Zheqi Chen<sup>1</sup>, Li Cheng<sup>1</sup>, Soudeh Afsharian<sup>1</sup>, Wensong Weng<sup>1</sup>, George A.  
4 Isaac<sup>1,2</sup>, Terry W. Bullock<sup>3</sup>, Yongsheng Chen<sup>1</sup>

5 <sup>1</sup> Centre for Research in Earth and Space Science, Lassonde School of Engineering, York University, Toronto,  
6 Ontario, M3J 1P3, Canada

7 <sup>2</sup> Weather Impacts Consulting Incorporated, 20 Pine Ridge Trail, Barrie, Ontario, L4M 4Y8, Canada

8 <sup>3</sup> Met-Ocean & Digital Environment Solutions, 133 Crosbie Road, St. John's, NL, A1B 4A5, Canada

9 *Correspondence to:* Peter Taylor (pat@yorku.ca)

10 **Abstract** There have been many studies of marine fog, some using WRF and other models. Several model studies  
11 report over-predictions of near surface liquid water content ( $Q_c$ ) leading to visibility estimates that are too low. This  
12 study has found the same. One possible cause of this overestimation could be the treatment of a surface deposition  
13 rate of fog droplets at the underlying water surface. Most models, including the Advanced Research Weather Research  
14 and Forecasting (WRF-ARW) Model, available from the National Center for Atmospheric Research (NCAR), take  
15 account of gravitational settling of cloud droplets throughout the domain and at the surface. However, there should be  
16 an additional deposition as turbulence causes fog droplets to collide and coalesce with the water surface. A water  
17 surface, or any wet surface, can then be an effective sink for fog water droplets. This process can be parameterized as  
18 an additional deposition velocity with a model that could be based on a roughness length for water droplets,  $z_{0c}$ , that  
19 may be significantly larger than the roughness length for water vapour,  $z_{0q}$ . This can be implemented in WRF either  
20 as a variant of the Katata scheme for deposition to vegetation, or via direct modifications in boundary-layer modules.

## 21 1. Introduction

22 This study was initiated when it was found that predicting fog in areas offshore from Atlantic Canada using the  
23 NCAR/UCAR Weather Research and Forecasting model (WRF-ARW) was generally satisfactory in terms of fog  
24 occurrence but gave high values of cloud water mixing ratio leading to visibilities that were too low compared to  
25 observations. Other studies of marine fog had encountered similar problems (e.g. Chen et al 2020). Koraćin et al  
26 (2014) had noted "From the many modeling studies of sea fog, essentially numerical experiments/ simulations/  
27 forecasting that started in the immediate post WWII period, it becomes clear that deterministic forecasting of sea fog  
28 onset and its duration has generally been unsuccessful.". On land and over the sea the formation and decay of fog in  
29 the atmospheric boundary layer is a complex issue involving many processes including cloud microphysics, long wave  
30 and solar radiation, turbulent boundary layer mixing, advection and surface interactions. Modelling of fog, in idealized  
31 one dimensional or single column models up to operational 3-D weather prediction and climate models is a challenge  
32 which many have addressed over the years, as noted by Koraćin (2017), Gultepe et al (2017) and many others. Koraćin  
33 et al (2014) review marine fog processes and studies up to 2014, noting the importance of air-sea interactions. They  
34 discuss fog water deposition to vegetation extensively but not turbulent deposition to water surfaces, and it is missing

35 from their Fig 1 (and Fig 9.1 in Koraćin 2017) showing " the main processes governing the formation, evolution, and  
36 dissipation of marine fog". Although fog could be caused by mixing two slightly sub-saturated air parcels and causing  
37 saturation due to curvature of the saturated mixing ratio versus temperature line, most fog formation is initialized by  
38 cooling the lower parts of a column of moist, but unsaturated, air. This can arise because of long wave radiative heat  
39 loss from the underlying surface (radiation fog), vertical displacement of the air column as it travels over sloping  
40 terrain or horizontal advection over a cooler surface. Our focus is on the advection fog situation over ocean waters, a  
41 frequent occurrence over areas such as the Grand Banks and offshore areas of Eastern Canada as the wind blows moist  
42 air from over the Gulf Stream towards the Labrador current (Taylor 1917; Isaac et al 2020).

### 43 1.1 Fog and the underlying surface

44 The focus in this paper is on the interactions of fog water droplets with the underlying water surface, how this is being  
45 modelled, how it could be improved in the widely used WRF model, and to briefly suggest some field measurements  
46 to support this work. The basic hypothesis will be that, in addition to gravitational settling, turbulence will induce  
47 collisions between fog droplets and the water surface and that most of these collisions will lead to coalescence, so that  
48 the water surface is a sink for water droplets. This can be represented in terms of a deposition velocity, over and above  
49 the settling or terminal velocity associated with small cloud droplets falling through air under gravity and predictable  
50 assuming Stokes law (see, for example, Rogers and Yau 1989). *Different authors use different symbols ( $Q_c$ ,  $q_w$ ,  $LWC$ ,  
51  $w$  etc.) and different measures ( $\text{g kg}^{-1}$ ,  $\text{kg m}^{-3}$  etc.) of fog or cloud water content. We will use  $Q_c$  for mixing ratio ( $\text{g}$   
52  $\text{kg}^{-1}$  or  $\text{kg kg}^{-1}$ ) and  $LWC = \rho_a Q_c$ , where  $\rho_a$  is air density, as liquid water content ( $\text{kg m}^{-3}$  or  $\text{g m}^{-3}$ ) unless discussing  
53 results from specific papers where, for clarity, it is sometimes useful to use their symbols. If there is an enhanced  
54 turbulent deposition to the water surface one would then expect the cloud water droplet mixing ratio ( $Q_c$ ) to approach  
55 zero at the surface and increase with height ( $z$ ) above the surface, at which  $Q_c$  would approach zero. In a constant  
56 flux layer this would lead to a logarithmic profile and allow the concept of a roughness length for cloud droplets,  $z_{0c}$ ,  
57 although the profile can be modified to incorporate gravitational settling (Taylor, 2021). Not included is the possible  
58 creation of spray droplets by breaking waves in high wind speeds, and this may need consideration in high seas with  
59 strong winds.*

60  
61 There have been many studies on the collision and coalescence of raindrops and cloud droplets, and of droplets  
62 impacting hydrophobic surfaces but relatively few concerning interactions between cloud or fog droplets and ocean  
63 surfaces. Over water the combination of wind and waves will lead to impacts occurring at a range of speeds and  
64 incidence angles and relatively little is known about the details of this important interaction. The paper by Hallett and  
65 Christensen (1984) and the reference to it by Isaac and Hallett (2005), although primarily on impacts at normal  
66 incidence, do however support our expectation that fog droplets interacting with the ocean surface are likely to  
67 coalesce eventually even if they may bounce on initial impact if that occurs at a shallow angle. If fog droplets do  
68 collide with the underlying surface, whether it is the ocean, a lake, a water puddle on land or wet vegetation one would  
69 expect coalescence and deposition of the fog droplets to the surface. Gravitational settling will play a role in this but  
70 droplet impacts on the surface due to turbulence also need to be considered. As a result of deposition there would be

Formatted: Font: Italic

Formatted: Font: Italic

Formatted: Font: Italic, Subscript

Formatted: Font: Italic

Formatted: Font: Italic

Formatted: Font: Italic, Subscript

Formatted: Superscript

71 a reduction in the fog/cloud water mixing ratio ( $Qc$ ), maybe to zero, at the lower boundary which would lead to a  
72 positive value for  $dQc/dz$  and a downward flux of  $Qc$ .

### 73 1.2 Aerosol and vegetation

74 If we broaden our view and consider aerosols in general, we find that significant work has been done in the same size  
75 range as fog droplets (1-50  $\mu\text{m}$ ). Recent reviews by Emerson et al (2020) and Farmer et al (2021) make it very clear  
76 that dry deposition (i.e. not rainfall related) of aerosol particles, solid or liquid, is a key process for their removal, that  
77 it is driven by turbulence and strongly dependent on particle size. For aerosol with diameters  $> 1 \mu\text{m}$  gravitational  
78 settling and turbulent diffusion both contribute to the overall deposition velocity. The aerosol studies include both  
79 water surfaces and vegetation. It is clear from Farmer et al (2021, Fig 3) that deposition velocity,  $V_{dep}$ , over water  
80 increases significantly with aerosol diameter between 1 and 50  $\mu\text{m}$ , while this variation is somewhat less over other  
81 surfaces. Farmer et al's plots are not normalized by friction velocity or wind speed which probably accounts for some  
82 of the variability in  $V_{dep}$  at fixed diameters.

83  
84 There have been studies of fog deposition to vegetation and also to meshes designed to catch fog water (e.g. Section  
85 3.4 of Gultepe et al 2017). However, as far as we are aware, the models of fog droplet deposition to water surfaces  
86 have either been via gravitational settling alone, ignored, or considered as a part of a turbulent, total water (vapour,  $q$ ,  
87 plus liquid droplets) flux at the surface. Right at the surface the flux of water vapour will rely on molecular transfer  
88 alone while collision and coalescence of water droplets can be much more efficient and requires separate treatment.

## 89 2 Boundary-Layer modelling

90 For aerosols and sometimes other quantities, weather prediction, and other models tend to use deposition velocities  
91 ( $V_{dep}$ ), to relate fluxes to an underlying surface to concentrations at some level above the surface. From a boundary-  
92 layer perspective, one often looks at the concentration profile and an eddy diffusivity. The simplest, and traditional,  
93 way to model flux-profile relationships of a quantity,  $s$ , in neutrally-stratified, turbulent boundary-layer flow near  
94 rough walls is via an eddy viscosity/diffusivity,  $K_s(z) = k u_* (z + z_{0s})$ , where  $k$  is the Karman constant (0.4) and  $u_*$  is the  
95 friction velocity. The roughness length,  $z_{0s}$ , is specific to the property (horizontal velocity, temperature, mixing ratio,  
96 ...) under consideration and will vary considerably depending on the physics of the final transfer process at the surface.  
97 The traditional way to determine  $z_{0s}$  is to consider an approximately constant flux layer near the surface - leading to a  
98 logarithmic profile,

99  
100  
101 
$$S - S_0 \approx (s*/k) \log(z/z_{0s}),$$
  
102 (1)

Formatted: Justified

Formatted: Justified

104 where  $S_0$  is the surface value. This will imply that  $S = S_0$  at  $z = z_{0s}$  and is the empirical way in which  $z_{0s}$  can be  
 105 determined. It is well known, see for example Garratt (1992, p 89) or Brutsaert (1982, p 121) that roughness lengths  
 106 for momentum ( $z_{0m}$ ) and heat or water vapour ( $z_{0T}$ ,  $z_{0q}$ ) transfers differ because form drag on roughness elements is  
 107 the major cause of momentum transfer while molecular diffusivity at the surface is needed to effect heat transfer. As  
 108 a result,  $z_{0m} \gg z_{0q}$ , except maybe over ~~very smooth~~ aerodynamically smooth surfaces. We will propose the use of  $z_{0c}$   
 109 for cloud droplet collision and coalescence with the water surface. We have no measurement data to determine a value,  
 110 which might well vary with droplet size and sea state but can use reported aerosol studies to provide some guidance.  
 111 We do however expect that  $z_{0c} \gg z_{0q}$ .

112  
 113 If the fog has continued for some time one might expect that the relative humidity,  $RH = 100\%$  in the fog layer, with  
 114 no significant condensation or evaporation. There will then be a near steady state in the lower fog layers with constant  
 115 downward  $Q_C$  flux ( $F_{Q_C}$ ). This flux will be a combination of turbulent diffusion and gravitational settling ( $w_s Q_C$ ) where  
 116  $w_s$  is the gravitational settling velocity, based on Stokes law. If, as we will assume,  $Q_C \rightarrow 0$  as  $z \rightarrow 0$  then turbulent  
 117 transfer will dominate as the surface is approached and logarithmic  $Q_C$  profiles should result.

118 In our model calculations, with an eddy diffusivity,  $K_e(z) = ku_*(z+z_{0c})$ , we do find  $RH \approx 100\%$  in the fog layers,  
 119 typically up to around 100m, and see constant flux layers with near-logarithmic  $Q_C$  profiles through most of this height  
 120 range, as in Fig 4. Departures from logarithmic could arise due in part to the effects of gravitational settling ~~which~~  
 121 ~~accounts for part of the downward flux.~~

122  
 123 Marine fog in the areas under consideration ~~is often~~ occurs in moderate and high wind conditions (Isaac et al, 2020).  
 124 ~~and~~ relatively low heights ( $< 10m$ ) are used as the lowest model level and i- In that lowest, constant flux, "wall"  
 125 layer with neutral stratification, we can assume horizontal homogeneity, a constant downward flux of  $Q_C$  and a steady  
 126 state. We can then seek the solution to

$$127 \quad w_s Q_C + (ku_*(z + z_{0c}) dQ_C/dz = F_{Q_C} = u_* q_{cs}, \quad (2)$$

128  
 129 where  $F_{Q_C}$  is a downward flux of cloud droplet liquid water mixing ratio and  $q_{cs}$  is introduced as a mixing ratio scale.  
 130 With  $Q_C = Q_{C0}$  at  $z = 0$ , the solution is,

$$131 \quad Q_C(z) - Q_{C0} = (u_* q_{cs} / w_s) [1 - \exp(-w_s \zeta / (ku_*))], \text{ where } \zeta = \ln((z + z_{0c}) / z_{0c}). \quad (3)$$

132  
 133 If  $w_s / u_*$  is small, then to first order in  $w_s \zeta / ku_*$ , (3) becomes simply

$$134 \quad Q_C(z) - Q_{C0} = (q_{cs} / k) \ln((z + z_{0c}) / z_{0c}), \text{ with } Q_C = Q_{C0} \text{ at } z = 0. \quad (4)$$

135  
 136  
 137  
 138  
 139 If this is used to relate  $z_{0c}$  to a deposition velocity,  $V_{dep}$ , and with  $Q_{C0} = 0$  we would have

140

Formatted: Font: Italic  
 Formatted: Font: Italic, Subscript

$$V_d = u_* k / (\ln((z_I + z_{0c})/z_{0c})), \quad (5)$$

where  $z_I$  is the height above the surface where  $Q_c$  is measured. This logarithmic profile approximation could be fit to measured  $Q_c$  profiles to determine  $z_{0c}$  from observations. As with  $z_{0m}$  this is a somewhat empirical approach. In the same way that the use of the  $z_{0m}$  concept is widely accepted without precise calculation of the form drag on roughness elements we would hope that future experimental determination of  $z_{0c}$  would be a way to account for the effects of turbulent collision and coalescence of fog droplets with a water surface. For radiation fog in low wind speeds over land, stable air density stratification effects could be significant and can be accounted for with Monin-Obukhov similarity modifications to  $K_c(z, L)$  if the Obukhov length ( $L$ ) can be determined.

The expected values of terminal velocity,  $w_s$  for a droplet of diameter,  $d$ , and density  $\rho$ , falling under gravity ( $g$ ) through air of density  $\rho_a$  and molecular viscosity,  $\mu$ , should be considered. In reality the fog droplet size distribution will be broad and often bimodal (see Isaac et al 2020). The two peaks in some of Isaac et al's measured PDFs are at diameters near 6  $\mu\text{m}$  and 25  $\mu\text{m}$  with Stokes law terminal velocities ( $w_s = gd^2(\rho - \rho_a)/\mu$ ) of 0.001  $\text{ms}^{-1}$  and 0.019  $\text{ms}^{-1}$ . These are clearly small compared to wind speed but for the larger diameter, where the bulk of the liquid water content (LWC) is often measured, the terminal velocity corresponds to 67 m per hour and will represent a considerable removal rate in fog which may last several days. The key parameter in our constant flux with gravitational settling model is  $S = w_s/ku_*$ . In moderate winds over the ocean one might expect  $u_*$  values in the 0.1-0.5  $\text{ms}^{-1}$  range,  $k = 0.4$  and so the parameter,  $S$  will generally be in the range 0.006 to 0.46 while  $\zeta$  may be 5-10 at the lowest grid point, implying that gravitational settling can play a significant role and that Eq. (3) may provide a more appropriate profile for the larger droplets. In principle Eq. (3) should be used to refine any  $z_{0c}$  estimates from measurements. For typical friction velocities (0.1 - 0.5  $\text{ms}^{-1}$ ) and with the lowest model level at  $z_I = 1.7$  m with  $z_{0c} = 0.001$  or 0.001 m,  $V_d$  values would be in the range 0.005 to 0.04  $\text{ms}^{-1}$ , quite comparable with the gravitational settling velocities so both will play a role in the modelling of deposition to the surface. [A more detailed analysis is presented in a companion ACP discussion paper, Taylor \(2021\).](#)

Ideally values for  $z_{0c}$  would be established from field measurements BUT we are not aware of any height profiles of  $Q_c$  in fog over water and for now will treat  $z_{0c}$  as a tuning parameter in our models. Over most land surfaces, [the surface roughness length for momentum](#),  $z_{0m}$  is considered independent of Reynolds number and we might hope that the same would apply for  $z_{0c}$ . Over water surfaces, with ripples and waves as the roughness elements, life gets more complicated and ~~the roughness length for momentum~~,  $z_{0m}$ , can be wind speed dependent, governed by the Charnock-Ellison relationship<sup>1</sup> (Charnock 1955),  $z_{0m} = au_*^2/g$ , where  $a$  is referred to as Charnock's constant, with typical values in the 0.01 - 0.03 range [and  \$z\_{0m}\$  values in the 0.05 to 1.5 mm range](#). Establishing precise over water values for  $z_{0c}$  will prove at least as difficult as for  $z_{0m}$ , noting that it may also vary with droplet size, but it does provide a framework for representing this potentially important fog deposition process.

<sup>1</sup> Henry Charnock always told me that Tom Ellison had suggested the dimensional analysis behind what is generally referred to as the Charnock relationship, so I refer to it in this way. - Peter Taylor

Formatted: Subscript

176 **3. Past Field and Laboratory Measurements**

177 There have been many field measurements in marine fog, including, notably, G.I. Taylor's (1917) work over the Grand  
178 Banks, and more recently the C-Fog study reported by Fernando et al (2021). As far as we are aware none have  
179 provided the  $Q_c(z)$  profile data from which we could make  $z_{0c}$  determinations.

180  
181 Over land there are some multi-level  $Q_c$  measurements indicating lower values near ground than above. Also lower  
182 droplet numbers. Kunkel (1984) reports measurements of advection fog in July 1980 and July 1981, at 2 levels (5m  
183 and 30m) on a tower "in the middle of a large, flat, open area" about 12 km inland from the Atlantic on Cape Cod.

184 There is some variability but his liquid water content values ( $W$ ,  $\text{g m}^{-3}$ ) are always higher at 30m than at 5m and the  
185 ratios are generally between 2 and 3. There are some differences in droplet size between the levels but they are  
186 relatively modest and less consistent. Ignoring stratification effects, assuming that a logarithmic profile is appropriate  
187 and that  $Q_{c0} = 0$  then the ratios of 2 and 3 in  $Q_c$  correspond to  $z_{0c}$  values of 0.833 m and 2.04 m. If  $Q_{c0}$  were  $> 0$ , say  
188 some fraction of  $Q_c(5\text{m})$ , then the  $z_{0c}$  values would be higher. Pinnick et al (1978) report  $Q_c$  measurements, from  
189 February 1976 above an inland site in Germany, at multiple heights up to 180 m with light scattering instruments  
190 carried aloft by a tethered balloon. Water content was calculated from particle size distributions and, from their  
191 photographs, the local land surface appears open and flat. Their sample profiles, in fog and haze, generally show  $Q_c$   
192 increasing with height and 3 of 4 cases shown are consistent with increases by factors of 2-3 between 5 - 30 m. Most  
193 of their results appear to be in radiation fog with light wind conditions. Klemm et al (2005) report eddy covariance  
194 measurements of fog water fluxes to a spruce forest at Waldstein, in a mountainous area of Bavaria Germany, and  
195 compare results with related model studies. They report that "turbulent exchange ...dominates over sedimentation at  
196 that site" and investigate relationships between liquid water content ( $LWC$ ,  $\text{g m}^{-3}$ ) and visibility. Their flux model is  
197 based on a deposition velocity,  $V_{dep}$ , with deposition to the canopy,

198  $F_{tot} = V_{dep} Q_c - LWC$ , including both turbulent flux and gravitational settling. They note that some studies at the same  
199 location (Burkhard et al, 2002) report significant differences in downward flux at different levels (flux at 22m can be  
200 45% less than at 35m), perhaps illustrating the difficulty of making representative measurements close to the canopy  
201 top. Evaporation of fog droplets is also cited as a possible cause of these differences. It is perhaps also worth adding  
202 that fog water collectors (e.g. Schemenauer and Cereceda, 1991) can enhance the amount of fog water that is removed  
203 at ground level and provide an important source of clean water for some isolated communities. a removal efficiency  
204 of 20% is estimated for a 2-layer, 12m x 4m polypropylene mesh.

205  
206 Turning to aerosol studies, Farmer et al (2021) provide an extensive list of laboratory and field studies of aerosol  
207 deposition to both land (grassland, forest, snow and ice) and water surfaces. Many provide  $V_{dep}$  values for aerosols in  
208 our size range. Deposition velocity measurements in wind tunnel studies in a short report by Schmel and Sutter (1974)  
209 are interesting, but lack details of how the aerosol flux to the surface was determined. From their Fig 3 we can estimate  
210 average deposition velocities for selected particle sizes and wind speeds. Unfortunately, it is not clear at what heights  
211 their wind speeds were measured and their  $z_{0m}$  and  $u_*$  values are somewhat suspect. If we assume that  $z_{0m} = 0.0002$  m  
212 and that wind speeds in their tunnel were measured at a height of 0.1 m then their average  $U$  ( $7.2 \text{ m s}^{-1}$ ) and  $u_*$  (0.44

213  $\text{m}_s^{-1}$ ) values are reasonably consistent and their  $V_{dep}$  value of  $0.04 \text{ m}_s^{-1}$  for  $6 \mu\text{m}$  diameter aerosol would lead to  $z_{oc} \sim$   
214  $10^{-4} \text{ m}$ . For larger diameter aerosol ( $28 \mu\text{m}$ )  $V_{dep} = 0.37 \text{ m}_s^{-1}$  and  $z_{oc} \sim 0.062 \text{ m}$  with the same wind assumptions,  
215 suggesting strong size effects, but we are wary of suggesting precise values.

216

217 Field data studies in the Farmer et al

218 2021) list include studies on Lake Michigan by Caffrey et al (1998) and Zufall et al (1998) with deposition to surrogate  
219 surfaces, and a recent report by Qi et al (2020) from the NW Pacific Ocean. These and other papers confirm the strong  
220 size dependence of deposition velocity and acknowledge wind speed dependence but are often concerned with long  
221 term estimates of the deposition of chemical species to the ocean or lake rather than short term events. One way in  
222 which wind speed plays a role is via wave breaking and "broken" water surfaces, a concept used in a model proposed  
223 by Williams (1982). This proposes that dry deposition of aerosol particles is considerable different between smooth  
224 and broken patches of the water surface with a much higher resistance over the smooth areas.

225

226 To briefly summarize we believe that there are observations to support the idea that the underlying land or water  
227 surface can be an effective sink for fog droplets, and other, similar sized, aerosol. The deposition velocity will have a  
228 dependence on droplet size, especially over water, but there is a lack of reliable data, even over land, to calibrate our  
229 simple, roughness length based approach to modelling the turbulent deposition of fog droplets. Our roughness length,  
230  $z_{oc}$ , will have to remain as a tuning parameter until more extensive fog droplet profile and flux measurements can be  
231 made.

#### 232 4. Model Studies

233 As reported by Koraćin (2017), there have been many studies aimed at understanding and/or predicting the occurrence  
234 of fog, and Kim and Yum (2012) also provide a review focused on marine fog. For our purposes it is relevant to see  
235 how different model papers discuss deposition of fog water to the surface and their surface boundary conditions on  
236  $Q_c$ . The model of Brown and Roach (1976) focusses on radiation fog, in relatively low wind speeds and provides an  
237 excellent summary of the key components needed to model fog formation and its life cycle, including radiation,  
238 turbulent diffusion and gravitational settling. They note that "liquid water (as well as water vapour) is also lost to the  
239 ground by turbulent diffusion and gravitational settling of droplets." and their lower boundary conditions include  $w =$   
240  $0$  for  $z = 0$  and  $t > 0$ , where  $w$  is their liquid water mixing ratio. Brown and Roach assert that " $K_h, K_q, K_w$ , exchange  
241 coefficients for heat, water vapour and liquid water ( $w$ ) respectively" are assumed equal in their model. In adiabatic  
242 conditions they state  $K = kz u_s$ , but avoid discussion of roughness length. Extrapolating their liquid water,  $w$  vs  $\log z$   
243 profiles to  $w = 0$  would indicate a  $z_{oc}$  value, for liquid water, of slightly less than  $10^{-2} \text{ m}$ . This is consistent with their  
244 use of the  $K$  model of Zdunkowski and Barr (1972) who set  $z_0 = 1 \text{ cm}$ . Zdunkowski and Barr's treatment of the  
245 conservation equation and lower boundary condition for  $M$ , the total moisture content (vapor plus droplets), plus zero  
246 flux of  $M$  to the surface, generally leads, inappropriately, to liquid water profiles with maxima at the surface. Barker  
247 (1977) developed a similar model for maritime boundary-layer fog and also uses the same eddy diffusivity and

248 roughness length for heat, water vapour and liquid water. He assumes [\(Barker 1977, Eq 19\)](#) that cloud liquid water  
249 concentration (his  $l_0$ ) is zero at the water surface.

250  
251 The COBEL and COBEL-ISBA 1-D models developed in France (Bergot 1993; Bergot and Guedalia 1994; Bergot  
252 et al 2005), have been used successfully at Paris's Charles de Gaulle International Airport. Bergot and Guedalia (1994,  
253 hereafter referred to as BG) provide details of dew and frost deposition to the underlying surface and note its  
254 importance. However their dew flux is based on direct condensation of water vapour to the surface (BG Eq 22) as the  
255 inverse situation of evaporation. Their liquid water ( $q_l$ ) diffuses and has a gravitational settling velocity (BG Eq 17,  
256 18) but no surface condition is specified and one assumes that the only flux to the surface is through gravitational  
257 settling. Few details are given on the surface boundary conditions in the latest journal publications but contour plots,  
258 e.g. Fig 13c from Bergot et al (2005) generally show  $Q_c$  maxima at the surface. COBEL has also been coupled with  
259 WRF (Stolaki et al 2012) and used to simulate advection-radiation fog conditions at Thessaloniki's airport. [Ducongé  
260 et al \(2020\) report on recent radiation fog modelling studies with Meso-NH downscaled from the Météo-France  
261 operational model, AROME.](#)

262  
263 Bott and Trautmann (2002) proposed PAFOG as "a new efficient model of radiation fog" and it has been used by  
264 others, including, recently, and coupled to WRF, in a study by Kim et al (2020). PAFOG is a 1- dimensional ( $z,t$ )  
265 model developed as a more practical version of the more complete MIFOG model (Bott et al 1990) which carries  
266 multiple aerosol and size bins for fog droplets. The MIFOG model includes dynamics and thermodynamics but  
267 focusses on interactions of radiation (solar and long wave) with fog droplets of varying size. The cloud droplets that  
268 evolve in the model have a bimodal size distribution which varies with time with large droplets descending under  
269 gravity, and being removed at the surface, at a faster rate than the small ones. The dynamics include turbulent mixing  
270 via eddy diffusivities for momentum and heat. Water droplet number concentrations in each size bin are also subject  
271 to diffusion with the same diffusivity as heat. The diffusivities are given by Forkel et al (1987). It appears that a  
272 common roughness length,  $z_0 = 0.05\text{m}$ , is used for momentum, heat and water droplets. No boundary conditions are  
273 given in Bott et al (1990) but from the results presented it would appear that there is no turbulent flux to the surface,  
274 only deposition via gravitational settling in MIFOG. The same appears to be true with PAFOG apart from possible  
275 removal of cloud water by vegetation as described by Siebert et al (1992a,b). PAFOG appears to give good results for  
276 2-m visibility (Bott and Trautmann 2002, Fig. 1). Their Fig. 2 generally shows high  $Q_c$  values ( $0.2, 0.3 \text{ g kg}^{-1}$ )  
277 extending almost down to the surface but with a sudden drop near  $z = 0$  in 3 of the 4 contour figures shown. There is  
278 similar near-surface behavior of  $Q_c$  in Siebert's results but it is not clear why. All of the above papers have a lack of  
279 detail on surface boundary conditions.

280  
281 Shuttleworth (1977) and later Lovett (1984) were early modelers of fog deposition to vegetation, using resistance  
282 concepts ( $L/V_d$ ). Katata et al (2008) later developed a land surface model (mod-SOLVEG) including fog and cloud  
283 water deposition on vegetation and on forests. The downward flux of cloud water is due to both turbulent mixing and  
284 gravitational settling (Katata 2014) and Katata et al (2008) successfully compare their model predictions with field



322 in terms of a flux to the surface but their results (Fig 3 of their paper) in a simulation of advection fog show number  
323 densities that are maximum at the fog top, around 30 m after 10 h, while  $Q_c$  and mean droplet radius are maximum  
324 near the ground.

325  
326 None of the papers that we have found use the  $z_{oc}$  approach that we have adopted, although the resistance and  
327 deposition velocity ideas of Lovett (1984), and Katata et al (2008) and Mazoyer et al (2017) are closely related. When  
328 roughness lengths are used, the values for  $Q_c$  always appear to be the same as for water vapour.

## 329 5. Operational NWP models

330 Fog forecasts have been a challenge for operational NWP models as indicated by many authors including Wilkinson  
331 et al (2013) who note the Gultepe et al (2006) opinion that "most NWP models were unable to provide accurate  
332 visibility forecasts, unless they accounted for both liquid water content and droplet number." We also note the  
333 comment of Bergot et al (2007), "Current NWP models poorly forecast the life cycle of fog, and improved NWP  
334 models are needed before improving the prediction of fog".

335  
336 Wilkinson et al (2013) focus on the droplet number issue and, in a somewhat "ad hoc" fashion, the UK Met Office  
337 Unified Model (MetUM) at that time applied "a taper curve for cloud droplets near the surface." This reduces droplet  
338 numbers between the surface and 150m without changing liquid water concentration. Droplets are then larger, have  
339 higher settling velocities and so "the impact ... is greatest closest to the surface, where they increase the amount of  
340 ( $Q_c$ ) removed from the lowest model levels." [Boutle et al \(2016, 2018\)](#) and [Smith et al \(2021\)](#) have adjusted the  
341 [MetUM taper parameters and obtained improved matches with visibility observations of fog, including the LANFLEX](#)  
342 [\(Price et al., 2018\) study](#). It seemed to work as a "tuning parameter" but their "taper curve" approach could certainly  
343 be considered somewhat "unphysical".

344  
345 Yang et al (2010) made an evaluation on the Canadian GEM-LAM model for marine fog off the east coast of Canada  
346 with nesting down to 2.5 km, using both visibility reports and  $Q_c$  comparisons with observed measurements from the  
347 FRAM project (Gultepe et al 2009). Three case studies are presented with the overall conclusion that GEM-LAM  
348 forecasts at 2.5 km resolution underestimate  $Q_c$  and had a warm and dry mean bias at the lowest model level. This is  
349 opposite to our WRF studies which predict high  $Q_c$  values at low levels. An earlier evaluation by de la Fuente et al  
350 (2007) had reported that, "... It has been shown that the current operational 15 km regional GEM forecast is insufficient  
351 for forecasting (sea) fog." The GEM-HRDPS (Milbrandt et al 2016) uses a MoisTKE treatment of the boundary layer  
352 which is described in Belair et al (2005). It works with the variable  $q_w = q_v + q_c$ , where  $q_c$  is the total cloud water  
353 content (droplets + ice fragments) which is mixed vertically using an eddy diffusivity  $K_H$ , as for heat. Assuming that  
354 surface transfers are of  $q_w$  this suggests no special treatment of cloud droplets over water surfaces. Milbrandt et al  
355 (2016) indicate that the cloud microphysics then used in GEM-HRDPS were based on MY2, the two-moment bulk  
356 microphysics scheme described in Milbrandt and Yau (2005). That paper includes the statement "... because cloud

357 droplets are assumed to have negligible terminal fall velocity." Fall speeds were given for different hydrometeor  
358 categories but not for fog droplets. As discussed above, terminal velocities under gravitational settling are small (mm  
359  $s^{-1}$ ), and can probably be considered negligible in a convective cloud but for long lasting marine fog they can play an  
360 important role. Currently GEM-HRDPS uses P3 microphysics (Morrison and Milbrandt, 2015). This includes  
361 gravitational settling of cloud droplets but there are subtle distinctions between explicit and implicit  $q_c$  from the  
362 microphysics and the boundary-layer treatments and there appears to be no surface flux of  $q_c$ , just a flux of  $q_i$ .

363  
364 Teixeira (1999) reported on ECMWF successes in fog forecasting at that time with the Tiedtke (1993) cloud scheme  
365 forecasting liquid water content. The Musson-Genon (1987) surface boundary-layer treatment treats diffusion of total  
366 water with a low surface roughness length, but includes gravitational settling of liquid water. Teixeira's conclusions  
367 include the statement, "The comparison between the simulated and the observed visibility shows that the onset of fog,  
368 the lowest values of visibility and the dissipation stage are properly simulated." In terms of marine fog in the Grand  
369 Banks area the reanalysis data showed that "The comparison between the model's fog climatology and the  
370 climatological data shows that the model is able to reproduce most of the major fog areas, particularly over the ocean."  
371 The ECMWF (2020) model physics are documented at [https://www.ecmwf.int/en/elibrary/19748-part-iv-physical-](https://www.ecmwf.int/en/elibrary/19748-part-iv-physical-processes)  
372 [processes](https://www.ecmwf.int/en/elibrary/19748-part-iv-physical-processes), with Chapter 3 giving information on interactions with the surface. As in our approach their transfer  
373 coefficients involve roughness lengths. Over water they specify  $z_{0m}$ , based on the Charnock-Ellison relationship plus  
374 a laminar flow value based on molecular viscosity ( $\nu$ ), while for moisture they specify  $z_{0q} = \alpha_q \nu / u_*$ , with  $\alpha_q = 0.62$   
375 (from Brutsaert, 1982), assuming simply molecular diffusion in a viscous sublayer. It is important to note that the  
376 ECMWF model deals with total water as a conservative variable,  $q_t = q + q_c + q_i$ , and that  $z_{0q}$  thus applies to water  
377 vapour, water droplets and ice fragments. The subscript "t" seems to be lost after Eq 3.3 in the ECMWF document but  
378 we assume that in what follows from that point, e.g. in their Eq. 3.6,  $q = q_t$ . Over land there are some adjustments but  
379 over water fluxes are proportional to  $(q_n - q_{surf})$  where  $q_n$  is at the lowest model level and  $q_{surf}$  is the surface value. The  
380 values of  $q_{surf}$  is set to  $0.98 q_{sat}(T_{sk})$ , where  $T_{sk}$  is the water surface "skin" temperature, implying that surface relative  
381 humidity is close to 100% AND that  $q_c \approx q_i \approx 0$ . This approximately agrees with our conjecture BUT the ECMWF  
382 model assumes the same  $z_0$  for water vapour and cloud droplets while our conjecture is that  $z_{0c} \gg z_{0q}$ . There is  
383 gravitational settling, with terminal velocities,  $v_t(D)$ , for rain and snow (their Eq 7.20, 7.21) but not for cloud droplets.

384  
385 In the USA there are many different forecast models but we will just consider the Rapid Refresh (RAP) and High  
386 Resolution Rapid Refresh (HRRR) Models, based on WRF-ARW, (Skamarock et al 2021). These are run  
387 operationally, with 13 km and 3km resolution meshes by NCEP and NOAA/ESRL Global Systems Laboratory. They  
388 use the same MYNN boundary-layer and Thompson microphysics modules as in our [marinecoastal](#) fog simulations  
389 and thus may have similar limitations in depositing fog droplets over water. Going back to a statement in Zhou and  
390 Du (2010), "Although one hopes that the liquid water content (LWC) at the lowest model level can be explicitly used  
391 as fog, experience indicates that an LWC-only approach does not work well with the current NWP models due mainly  
392 to two reasons: one is the too coarse model spatial resolution and the other is a lack of sophisticated fog physics."

393 Things have changed since then but the recent "somewhat improved" statement (including the qualifier, somewhat)  
394 on visibility performance by Alexander et al (2020) can be noted.

## 395 6. Fog deposition treatment in the WRF model with module\_bl\_mynn and module\_sf\_fogdes

396 WRF versions 4.1.2 and 4.2.1 (<https://www2.mmm.ucar.edu/wrf/users/downloads.html>), and possibly earlier  
397 versions, march forward in time with separate modules for dynamical and multiple physical processes (see Skamarock  
398 et al 2021; Olson et al 2019). For the benefit of readers familiar with, or interested in, the WRF model we provide  
399 some details, here, in Section 6 and in Cheng et al (2021a). The WRF modules used here treat gravitational settling  
400 and turbulent diffusion as separate processes and compute separate tendencies, including deposition rates.  
401 Gravitational settling is included within the Thompson microphysics module and, within the MYNN boundary layer  
402 module. Eq. (4) is used to compute deposition velocities associated with turbulent diffusion with  $V_d =$   
403  $u_*k/(\ln((z_1+z_{oc})/z_{oc}))$ , where  $z_1$  is the first Qc model level above the surface. The surface boundary layer is treated in a  
404 1-D implicit finite difference mode with tridiagonal matrices set up for turbulent kinetic energy, velocity components,  
405 potential temperature, humidity and cloud liquid water  $Qc$ . Variables are defined at the centres of grid cells with fluxes  
406 at the upper and lower boundaries. For the cells adjacent to the ground the fluxes at the cell upper-eefH surface use an  
407 eddy diffusivity ( $K$ ) approach, which for a downward flux of cloud water is of the form  $K(Qc(2)-Qc(1))/dz$  where  
408  $Qc(1)$  is the value in the centre of the lowest level grid cell and  $dz$  is the vertical separation. The turbulent flux to the  
409 lower boundary, in this case the water surface, is computed with a deposition velocity. For cloud water the (negative)  
410 upward flux is  $flqc$  and is computed in module\_bl\_mynn as  $-vdfg(Qc(1)-sqcg)$  with the deposition velocity  $V_d = vdfg$   
411 provided by module\_sf\_fogdes and with  $Qc$  on the surface,  $sqcg = 0$ . In the unmodified module\_sf\_fogdes, water  
412 surfaces are classified as "other" and the deposition velocity assumed is just the settling velocity of the cloud droplet  
413 falling through air under gravity. One must be careful not to double count gravitational settling in both the  
414 microphysics and boundary-layer modules. In a turbulent flow over a wavy water surface the deposition velocity  
415 should also include the effects of turbulence bringing droplets to impact the water surface and coalesce, and  $vdfg$   
416 should be higher. There are different ways in which this can be implemented in WRF module\_bl\_mynn (see Cheng et  
417 al, 2021a).

### 418 6.1 WRF SCM set-up and tests

419 As a basic test of our treatment of deposition of fog droplets to a water surface and for comparisons against the regular  
420 WRF schemes we use the single column version (SCM) of WRF (em scm xy), one of the ideal test cases described by  
421 Skamarock et al (2021). In our applications of this SCM we used several boundary layer and microphysics schemes,  
422 set up various vertical grids with up to 201 levels, and different lowest and upper levels. Initial soundings have close  
423 to 100% relative humidity in the lowest few hundred meters, moderate wind speeds typical of the NW Atlantic and  
424 WRF-SCM was typically run for 36 - 84 h. To simplify interpretation of the results, our SCM runs are without any  
425 solar or long wave radiation. Surface temperatures were cooled for several hours and then held steady. The main  
426 interest is to see the impact of fog ~~droplet~~-deposition to the underlying water surface. Physics and Dynamics

427 components of the WRF namelist input are listed in Cheng et al (2021a). Turbulent deposition to the surface is  
 428 represented via a deposition velocity,  $V_d$ , multiplying the lowest level  $Q_c$  value at  $z = z_l$ . This is set as

429

$$430 \quad V_d = ku_{*w} / \ln((z_l + z_{0c}) / z_{0c}), \quad \text{—————}$$

431 (87)

432

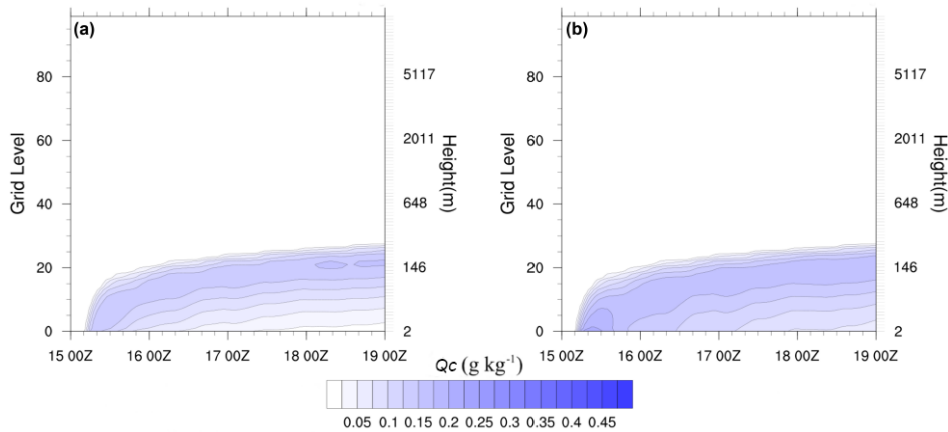
433 where  $u_*$  is the friction velocity,  $k (= 0.4)$  is the Karman constant and  $z_{0c}$  is a roughness length specific to water droplets  
 434 diffusing to a water surface and coalescing. In principle it could be dependent on sea state and droplet size. ~~As noted~~  
 435 ~~above, roughness lengths can represent different processes for turbulent transfers of heat, water vapour, momentum,~~  
 436 ~~and fog droplets of liquid water to the surface, and should not all be the same.~~ Our assumption is that  $z_{0c}$  (for fog/cloud  
 437 droplets) should be significantly larger than  $z_{0q}$  for water vapour.

438

439 WRF-SCM was run using modules bl\_mynn, for boundary-layer turbulent transfers, and mp\_thompson (with  
 440 mp\_physics=8), for cloud microphysics, to generate the results shown in Figs 1-3. Since gravitational settling is  
 441 represented within mp\_thompson the parameter grav\_settling was set to 0 in bl\_mynn (see Olson et al, 2019, section  
 442 6.4). No radiation effects are included. Lack of long wave radiation will affect mixing at the top of the fog layer but  
 443 we will focus on lower boundary issues. In the results below, the initial sounding has potential temperature of 300 K  
 444 at the surface increasing with height at a rate of 4 K km<sup>-1</sup>. The initial relative humidity was 100 % at the surface  
 445 dropping to 0 at 6 km. The wind profile was established with a long, no cooling run and has a geostrophic wind of  
 446 (20,0) m s<sup>-1</sup>. Sea surface temperature was cooled at a rate of 3 K h<sup>-1</sup> for 6 h and then held fixed. The lower boundary  
 447 condition included a flux of water droplets to the surface, computed with a deposition velocity determined by Equation  
 448 (8) above and using a range of  $z_{0c}$  values.

449

450



451

452

453  
454 **Figure 1: Contours of  $Q_c$  ( $\text{g kg}^{-1}$ ) generated by WRF SCM with 6 h of surface cooling at  $3 \text{ K h}^{-1}$  a) MYNN boundary layer**  
455 **using the turbulence deposition scheme described with  $z_{0c} = 0.01 \text{ m}$  plus Thompson microphysics with gravitational settling,**  
456 **b) Original MYNN module with gravitational settling only in Thompson microphysics. The full vertical domain is shown**  
457 **to indicate that no upper level cloud formed in these cases - it did with other input. Times on the x axis are in the format**  
458 **DD HHZ, with small tic marks 4 hours apart. Run start time was 15 00Z.**  
459

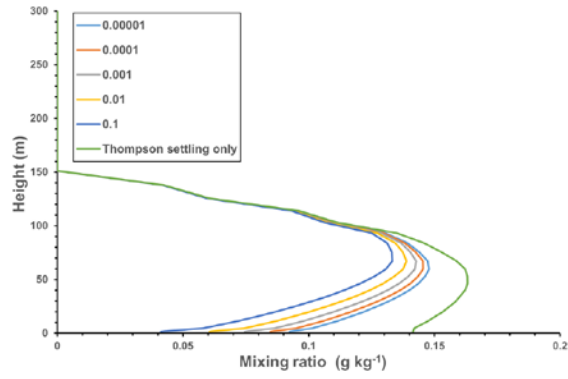
460  
461 Fig. 1 shows contours of  $Q_c$  ( $\text{g kg}^{-1}$ ) as it varies with ( $t$ , eta grid level) from the model calculations over 4 days starting,  
462 somewhat arbitrarily, at 00Z on day 15 of a month (15 00Z) so that cooling runs to 15 06Z. Some height  
463 levels are marked to indicate the grid stretching in  $z$ . These runs are for latitude  $44^\circ \text{ N}$  (Sable Island) with 101 eta grid  
464 levels. The WRF model operates with a sigma type vertical coordinate ( $\eta$ ), decreasing from 1 at the lower boundary  
465 to 0 at the upper boundary, where  $p = p_t$ . It has a simple form over a flat surface. Details are in Skamarock et al 2021).  
466 Our model grid points are not uniformly spaced in  $\eta$  and the spacing increases smoothly with increasing height  
467 (decreasing  $\eta$ ). We set  $p_t \approx 22000 \text{ Pa}$  to give a top boundary at about 12 km. The Eta levels start at  $\eta = 1$  (the surface)  
468 decreasing to  $\eta = 0$  and  $p = p_t$  at Eta level 101 (our SCM model top). In full 3D runs we take  $p_t = 5000 \text{ Pa}$ . The grid  
469 is staggered so that variables like  $\theta$ ,  $Q_v$ ,  $Q_c$ ,  $U$ ,  $V$ , where  $\theta$  is potential temperature and  $Q_v$  is the water vapour  
470 mixing ratio, are at mid-levels, while the lower boundary ( $z = 0$ ) is at the base of the lowest grid cell. Our 'grid levels'  
471 start with the center of the lowest cell (0) and increase upwards. In Fig. 1a,  $z_{0c} = 0.01 \text{ m}$  while Fig. 1b is for results  
472 with the original MYNN scheme with no surface deposition except for gravitational settling in the Thompson  
473 microphysics. Fog forms as a result of the surface cooling and extends from the surface to around eta level 20, which  
474 corresponds to  $z \approx 150 \text{ m}$ . We were initially concerned by the wave-like features in the contour lines. These have a  
475 period of around 17 h and arise because of inertial oscillations (of period  $2\pi/f$ ) in the wind field, ( $U, V$ ), as it adjusts to  
476 the cooling of the surface and changing turbulent momentum transfers. They decay slowly as the wind profile adjusts  
477 to the cooler surface. Values of  $Q_c$  are lower in Fig. 1a because of turbulent deposition to the surface. Fig. 2 shows  
478  $Q_c$  profiles with the MYNN boundary layer, at 16 00Z, 24 h after the start of the model calculations and 18 h after the  
479 end of surface cooling. The additional turbulent deposition can play an important role in lowering  $Q_c$  levels in the  
480 boundary layer while, in this case, not having a significant impact above 100m. The amount of the reduction depends  
481 on the value chosen for  $z_{0c}$ .

482

Formatted: Font: Not Italic

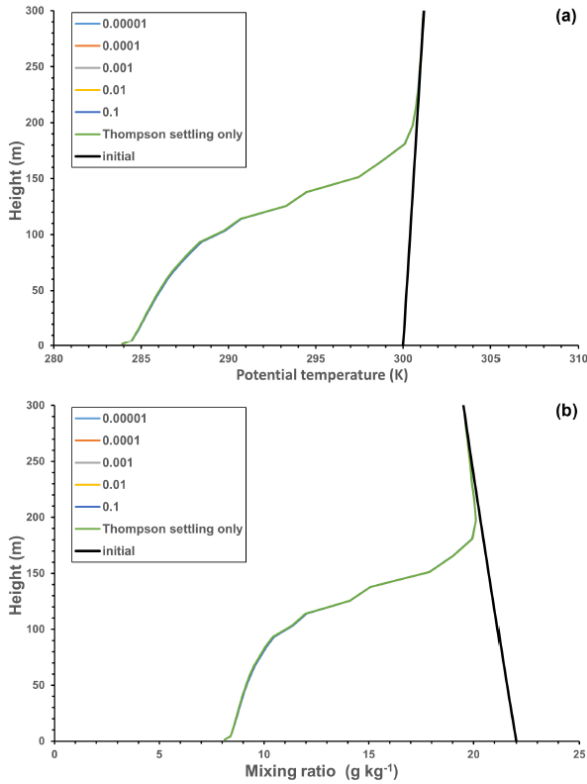
Formatted: Font: Not Italic

Formatted: Font: Italic



483  
 484  
 485  
 486  
 487  
 488  
 489

Figure 2:  $Q_c$  profiles 24 h after the start of the integration and 18 h after the end of the surface cooling, by 18 K. Results with the original MYNN (gravitational settling in Thompson microphysics only) and with a range of  $z_{0c}$  values (in m). Time step,  $dt = 60$  s, 101 levels.



490  
 491  
 492 **Figure 3: a) Potential temperature ( $\theta$ ) and b)  $Q_v$  profiles corresponding to Fig. 2, including the initial profiles. Note  $z_0$**   
 493 **deposition of cloud droplets has minimal impact, and**  
 494 **all curves overlay.**

495  
 496 It is interesting to note that the removal of  $Q_c$  at the lower boundary has minimal impact on the predicted temperature  
 497 and water vapour,  $Q_v$  profiles (Fig. 3). It could however be important when fog starts to evaporate if the air temperature  
 498 rises. Note that in generating these results we have not included radiation (short wave or long wave) effects in order  
 499 to focus on the impacts of turbulent deposition at the water surface. Radiation can play a significant role once fog has  
 500 formed, and in particular long wave radiational cooling at the fog top (Yang and Gao, 2020) can add to the cooling  
 501 rate and can enhance turbulent mixing in the upper part of the fog layer. The center of the lowest grid layer is at 1.7  
 502 m. Noting the "kinks" in the profiles at the lowest level in profiles of  $Q_c$ ,  $Q_v$  and  $\theta$ , we investigated possible causes  
 503 and plotted them on an expanded height scale (not shown). They arise because in WRF modules sf\_mynn and  
 504 sf\_fogdes the fluxes to the surface are computed with deposition velocities involving  $\ln((z+z_0)/z_0)$  while the eddy  
 505 diffusivities used to compute fluxes at the top of the first level and levels above are based on length scales proportional

506 to  $kz$  without the  $z_0$  addition. This will not be significant for  $z \gg z_0$  but with the lowest computational levels close  
507 to the surface this could be modified. This is an internal WRF issue, noted in comments within the module\_bl\_mynn  
508 module-code.

509  
510 A further point from Fig 3b is that with our near saturated initial profile and strong cooling there is a significant  
511 reduction in  $Q_v$ , of order  $10 \text{ g kg}^{-1}$  throughout the lowest 100 m. This will be converted to  $Q_c$  but after 24 h most will  
512 have been deposited to surface, through both gravitational settling, as in the "original" curves in Fig. 2, or by a  
513 combination of gravitational settling and turbulent deposition to the water surface as in the other cases shown in Fig.  
514 2. In runs with gravitational settling turned off in the microphysics (not shown for this case but see Fig 4b) and no  
515 turbulent deposition the  $Q_c$  values increase significantly, to around  $6 \text{ g kg}^{-1}$  near the surface after 12 h. This is not  
516 shown for this case but see the 3D case in Fig 4b, although then there is less cooling. Gravitation settling generally  
517 prevents very high  $Q_c$  values from occurring but additional turbulence induced deposition further limits them.

Formatted: Font: Italic

### 518 7. 3D test cases

519 Turning to the 3D WRF model, we have been running the model for North Atlantic simulations for summer 2018 on  
520 a domain extending from eastern Canada out beyond the Grand Banks and including Sable Island. A separate paper  
521 on comparisons with visibility measurements on Sable Island is in preparation while some sample results are in Cheng  
522 et al (2021b). These 3D runs have no additional surface cooling and are simply run as hindcasts of the actual situation  
523 with initial and boundary conditions taken from NCEP analyses. The sea surface temperatures are held fixed for daily  
524 36 h runs, generally with a 12 h spin up. Note that the input initial and boundary fields had zero  $Q_c$ . They are run with  
525 hybrid\_opt = 0, and in the vertical direction we have a straight "sigma" coordinate,

$$526 \eta = (p_t - p_s) / (p_r - p_s)$$

527  
528  
529 with  $p_t = 5000 \text{ Pa}$ . Runs were also made with hybrid opt = 2 and  $Q_c$  results were almost identical. Solar and long wave  
530 radiation can use either Goddard or RRTMG scheme and we used the MYNN PBL scheme with either the both  
531 Thompson ~~or~~ and the WSM6 microphysics options. For details of these options see Skamarock et al (2021). Figs. 4  
532 and 5 shows sample results from 6 h after the start of a runs with the full 3D model using Thompson microphysics  
533 and Goddard radiation, long and short wave.

534  
535 With 3-D WRF simulations we initially look at plots and animations over our d02 domain (see Cheng et al, 2021a) at  
536 the lowest model level. Fig 4 is an example of 2D plots of  $Q_c$  at the same time as in Fig 5, with and without turbulent  
537 deposition. The black dot identifies the Grand Banks location (GB) used in Fig 5. The value of  $z_{qc}$  was 0.01 m. In  
538 additional runs (not shown) with no gravitational settling the spatial fog patterns are similar but in the extreme case  
539 with no turbulent deposition the  $Q_c$  values are up to  $0.8 \text{ g kg}^{-1}$  in some areas although it is only  $0.4 \text{ g kg}^{-1}$  at our GB  
540 location.

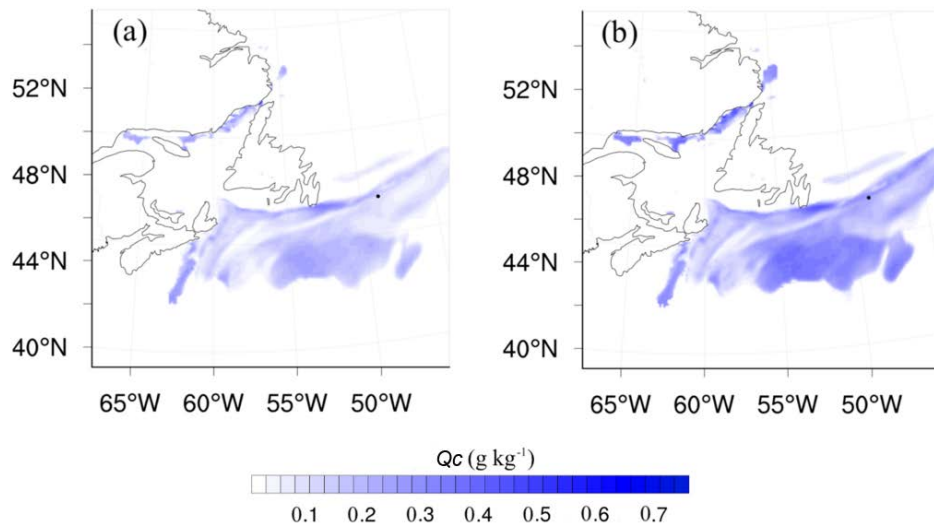
Formatted: Font: Italic

Formatted: Font: Italic

Formatted: Font: Italic, Subscript

Formatted: Font: Italic

Formatted: Superscript



541 **Figure 4. 2D fog plots at lowest model level, July 1, 18Z, 2018 from WRF. Thompson microphysics with gravitational**  
 542 **deposition, a)  $z_{0c} = 0.01$  m, b) no turbulent deposition, related to Fig. 5a. The black dot shows the point on the Grand Banks**  
 543 **that the profiles in Fig 5 correspond to.**  
 544  
 545

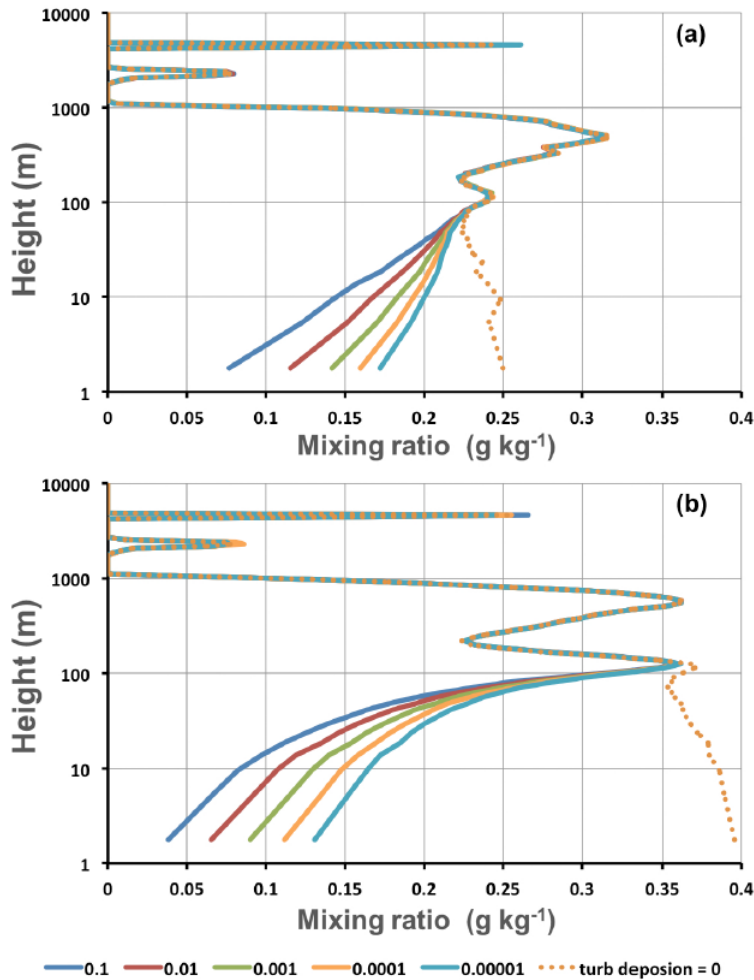
546 In Fig. 5 they the  $Q_c$  profiles show a similar response to the SCM (Fig. 2) when turbulent deposition of cloud water  
 547 to the surface is introduced. The top figure (54a) shows a normal run with the Thompson microphysics module  
 548 accounting for gravitational settling effects. MYNN has turbulent deposition to the surface but no gravitational settling  
 549 (grav\_settling = 0). In the lower figure (Fig. 54b) we removed gravitational settling from the Thompson microphysics  
 550 scheme (av\_c = 0) as well as from MYNN. With no turbulent deposition to the surface, and, in one special case with  
 551 no gravitational settling either, there are higher  $Q_c$  values as expected. These 3-D runs used NCEP analyses as initial  
 552 conditions but the initial  $Q_c$  was set to zero everywhere. In fog the analysis would give 100 % RH and the model then  
 553 generated  $Q_c$  within a few hours but without the strong temperature and  $Q_v$  drops that were simulated in our SCM  
 554 tests. Gravitational settling (Fig. 54a) has reduced the peak  $Q_c$  values at around 100 and 900 m from the case with no  
 555 settling and the  $Q_c$  removed from those levels has settled and mixed downwards to increase the  $Q_c$  values near the  
 556 ground.  
 557

558 Additional 3D runs were made with the standard MYNN codes and the Katata scheme using modified deposition  
 559 velocities in the "other" case. These matched our results obtained with a modified MYNN code. Also, in place of the  
 560 Thompson microphysics scheme we ran tests with WSM6 microphysics. In all cases there was a large impact of  
 561 turbulent surface deposition of  $Q_c$  in the lowest 100 m, even with very low values for  $z_{0c}$ . As an initial guide we  
 562 suggest using  $z_{0c} = 0.01$  m or 0.001 m as a modest value which has a solid impact. We should also emphasize that  
 563 gravitational settling also has an impact on  $Q_c$  values near the surface and both processes need to be included in  
 564 models.

**Formatted:** Font: (Default) Times New Roman, 9 pt, Bold, Italic

**Formatted:** Font: (Default) Times New Roman, 9 pt, Bold, Italic, Subscript

565  
566 ~~Additional 3D runs were made with the standard MYNN codes and the Katata scheme using modified deposition~~  
567 ~~velocities in the "other" case. These matched our results obtained with a modified MYNN code. Also, in place of the~~  
568 ~~Thompson microphysics scheme we ran tests with WSM6 microphysics. In all cases there was a large impact of~~  
569 ~~turbulent surface deposition of  $Q_c$  in the lowest 100 m, even with very low values for  $z_{0,c}$ . As an initial guide we~~  
570 ~~suggest using  $z_{0,c} = 0.01\text{m}$  or  $0.001\text{m}$  as a modest value which has a solid impact. We should also emphasize that~~  
571 ~~gravitational settling also has an impact on  $Q_c$  values near the surface and both processes need to be included in~~  
572 ~~models.~~  
573  
574



575  
576

577 **Figure 54:** Sample 3-D WRF output at a fixed location over the Grand Banks, with different  $z_{0c}$  values (given in m) in  $Q_c$   
578 turbulent deposition, a) with and b) without gravitational settling. Start time (month/day hour, year) was 7/1 12Z, 2018 and  
579 results are for 7/1 18Z. Results are with MYNN boundary layer and Thompson microphysics.

580 microphysics scheme we ran tests with WSM6 microphysics. In all cases there was a large impact of turbulent surface  
581 deposition of  $Q_c$  in the lowest 100 m, even with very low values for  $z_{0c}$ . As an initial guide we suggest using  $z_{0c} =$   
582 0.01 m or 0.001 m as a modest value which has a solid impact. We should also emphasize that gravitational settling  
583 also has an impact on  $Q_c$  values near the surface and both processes need to be included in models.

584 **8 Visibility considerations**

585 Models can predict liquid water mixing ratios but the critical forecast issue is visibility which will depend on the  
586 number and size distribution of the fog droplets. In dense marine fog ( $LWC > 0.05 \text{ g m}^{-3}$ ), Isaac et al (2020, Fig. 12)  
587 show that the size distribution of marine fog droplets is generally broad and frequently bimodal, raising concerns about  
588 all simple diagnostic schemes. Despite such concerns, models such as the one proposed by Isaac et al (2020) assume  
589 that visibility, ~~or Meteorological Optical Range, MOR~~ is proportional to ~~liquid water density, LWC ( $\text{g m}^{-3}$  or  $\text{kg m}^{-3}$ )~~  
590 ~~or mixing ratio ( $\text{g kg}^{-1}$  or  $\text{kg kg}^{-1}$ ),~~  $LWC^{2/3}$  times  $N^{1/3}$  where  $N$  is the droplet number density ( $\text{m}^{-3}$ ). Some models  
591 include dynamic equations for  $N$  while others assume prescribed values, typically  $N = 10^8 \text{ m}^{-3}$ . If the size distribution  
592 were well known and universal this could work but as Isaac et al (2020) note the size distribution in fog over the ocean  
593 can be bimodal and the number density can vary widely. In conditions with ~~air density  $\times Q_e$~~   $LWC > 0.005 \text{ g m}^{-3}$  the  
594 number density reported by Isaac et al over a site in the Grand Banks area varies between  $10^7$  and  $3 \times 10^8 \text{ m}^{-3}$ . Medians  
595 were close to  $N = 0.8 \times 10^8 \text{ m}^{-3}$ . Note however that these measurements were at a height of 69 m above the ocean surface  
596 and if the water surface is a sink for cloud droplets one would expect lower values, and maybe a different size  
597 distribution, at the WMO standard visibility measurement height of 2.5 m (WMO, 2020). Chen et al (2020) note  
598 problems with too low visibility from their WRF calculations coupled to the Kunkel (1984) visibility equation ( $vis =$   
599  $-\ln(\epsilon)/\beta$  with the extinction coefficient ( $\text{km}^{-1}$ ),  $\beta = 144.7 W^{0.88}$  where  $W$  ~~(or LWC) is in  $\text{g m}^{-3}$~~ ). The contrast threshold,  
600  $\epsilon$  was given as 0.02 by Kunkel but is set to 0.05, as recommended by the WMO (Boudala et al 2012; Chen et al 2020).  
601 In the GSD algorithm used in NCEP's Unified Post Processor version 2.2, the Kunkel result is used with  $\epsilon = 0.02$  for  
602 visibility reductions in clouds, plus additional effects of aerosol, rainfall and humidity. The relationship between  
603 visibility ~~or MOR~~ and  ~~$Q_e$  or  $LWC$~~  can vary in these models between a power of  $-2/3$ , through  $-0.88$  to  $-1$  if  $N$  were  
604 proportional to  ~~$Q_e$~~   $LWC$ , but all show that too high a value of  ~~$LWC$  or  $Q_c$~~  will lead to too much reduction in visibility.  
605 Running standard versions of WRF one can compute visibilities with either the Isaac et al (2020) equations or the  
606 GSD algorithm used in NCEP's Unified Post Processor version 2.2 (for details, see Lin et al 2017). Both led to  
607 significantly lower values of ~~MOR~~ visibility than were reported on Sable Island. Typical WRF values being of order  
608  $1/10 - 1/5$  of the reported visibility, suggesting  $Q_c$  values that may be high by a factor between 5 and 30. Visibility -  
609 cloud water relationships are open to revision, with different values of  $\epsilon$  and noting the scatter in Isaac et al's (2020)  
610 data, but there is a strong suggestion that WRF values of  $Q_c$  are too high without adding additional  $Q_c$  deposition.

611  
612 Fig. 6 shows sample visibility time series computed from 3D WRF  $Q_c$  output for the Sable Island location, vertically  
613 interpolated to  $z = 2\text{m}$ , for two 36 h periods in 2018 when fog was reported at Sable. We should however note that  
614 these computations were made with a 10 km horizontal mesh and there was no island. In reality the presence of a land  
615 surface can modify the temperature, up or down, leading to Relative Humidity, LWC and visibility adjustments as air  
616 travels in from the shoreline (see for example Cheng, 2021b). In these cases the fog occurred in daytime and  $Q_c$  could  
617 be lower at the weather station than offshore. Original WRF runs with just gravitational settling show seriously limited  
618 visibility ( $< 100\text{m}$ ) on some occasions when METAR visibility was closer to 1 km while with added turbulent  $Q_c$   
619 deposition and a range of  $z_{0c}$  values, the optical range was a better match to the observations. These are sample cases  
620 and a more extensive comparison is planned.

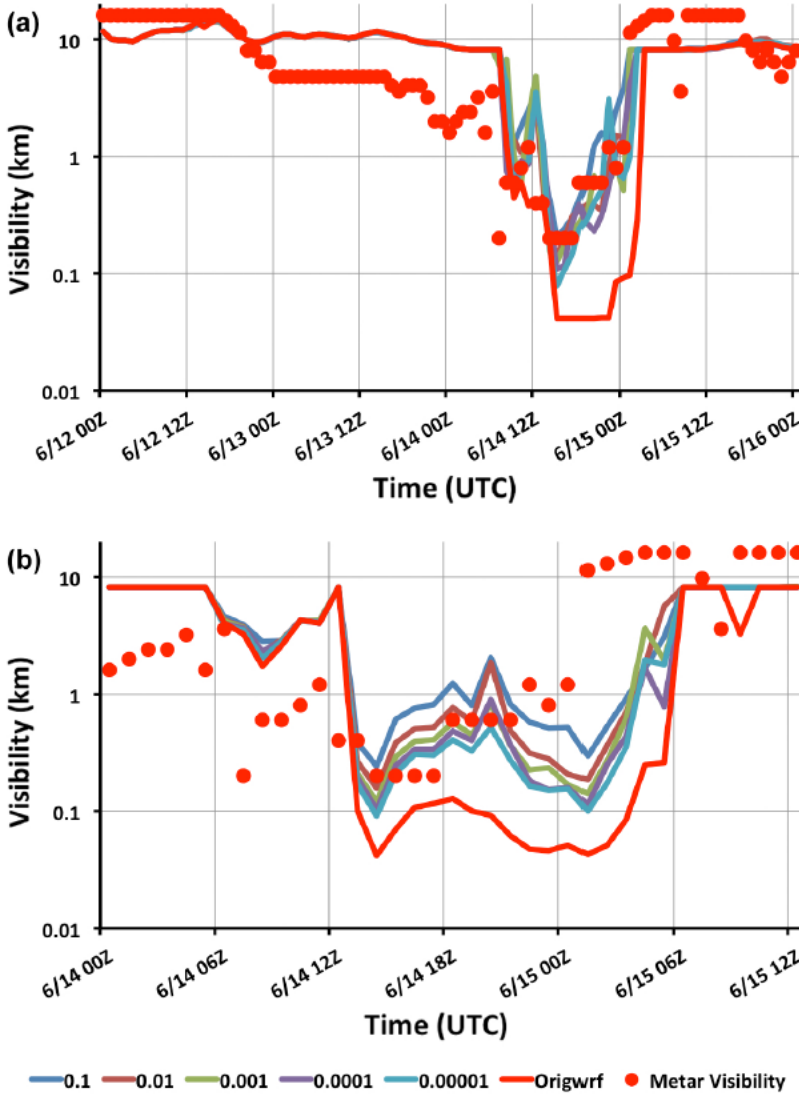
Formatted: Font: Not Italic

Formatted: Font: Not Italic

Formatted: Font: Italic

Formatted: Font: Italic

Formatted: Font: Italic



622 Fig.—5  
623 shows sample visibility time series computed from 3D WRF  $Q_c$  output for Sable Island, interpolated to  $z = 2m$ , for  
624 two 36 h periods in 2018 when fog was reported at that location. Original WRF runs with just gravitational settling  
625 show seriously limited visibility ( $< 100m$ ) on some occasions when METAR visibility was closer to 1 km while with

626 added turbulent  $Q_e$  deposition and a range of  $\varepsilon_{0c}$  values, the optical range was a better match to the observations. These  
627 are sample cases and a more extensive comparison is planned.

630 Figure 65: Sample June 2018 GSD visibility hindcasts for Sable Island at 2m, using MYNN boundary layer and WSM6  
631 microphysics, with different  $z_{0c}$  values, given in m.

## 634 9. Conclusions

635 It has been known for many years that fog water can be deposited on vegetation and this has been incorporated into  
636 some boundary-layer fog models. It is also known that  $\mu\text{m}$  size aerosols can be removed from the atmosphere by  
637 turbulence at water, and other, surfaces (Farmer et al, 2021). It then seems surprising that, for marine fog, turbulence  
638 induced cloud/fog droplet deposition to water surfaces has not been recognised by most modellers as a significant  
639 potential addition to the deposition associated with gravitational settling. Neglecting this can then lead to fog liquid  
640 water mixing ratios being too high and visibility forecasts being too low. This applies to specialised boundary layer  
641 models and to numerical weather prediction models. Many authors have noted the difficulties and complexity of  
642 modelling fog and accurately forecasting visibility. Getting everything right will be extremely challenging but, for  
643 marine fog, recognising that a significant process is missing from many models could be a step in the right direction.

644  
645 WRF-ARW is a major contribution to the atmospheric research endeavour and the developers and maintainers of this  
646 huge, multi-faceted, publicly available model deserve huge credit. As with anything of this size and complexity,  
647 developed and modified over many years by many individuals, it can be very hard for new users to trace through the  
648 source codes and understand just how they work. Some module codes are well documented and commented, others  
649 less so. Running the model is made relatively easy, and it is designed to be robust. We have done our best to understand  
650 some details and ensure that our modifications, briefly explained in Cheng et al (2021a), do what we expect but we  
651 make no guarantees!

652  
653 [Recent fog field programs including LANFEX \(Price et al., 2018\) in the UK, SoFog 3D \(https://www.umr-](https://www.umr-cnrm.fr/spip.php?article1086&lang=fr#outil_sommaire_0)  
654 [cnrm.fr/spip.php?article1086&lang=fr#outil\\_sommaire\\_0\)](https://www.umr-cnrm.fr/spip.php?article1086&lang=fr#outil_sommaire_0) in France and studies in India and China have focussed on  
655 [fog over land, but are providing valuable field data for model comparisons. The C-Fog campaign \(Fernando et al,](https://www.umr-cnrm.fr/spip.php?article1086&lang=fr#outil_sommaire_0)  
656 [2021\) is providing valuable data on coastal fog and the 2021-2026 Fatima \(Fog and Turbulence Interactions in the](https://www.umr-cnrm.fr/spip.php?article1086&lang=fr#outil_sommaire_0)  
657 [Marine Atmosphere, https://efmlab.nd.edu/research/Fatima/\)](https://www.umr-cnrm.fr/spip.php?article1086&lang=fr#outil_sommaire_0) project will be a major contribution to the understanding  
658 [of marine fog.](https://www.umr-cnrm.fr/spip.php?article1086&lang=fr#outil_sommaire_0)

659  
660 Based on our modelling of marine fog with WRF, and reviews of the treatment of boundary layer fog in WRF and  
661 other models, it seems that a ~~much~~ better understanding of fog droplet interaction with the ocean surface, and other

662 surfaces, is needed. Laboratory studies might be possible, and numerical simulations, but with some good in situ  
663 profile measurements through fog layers over land and water one could start to better understand and parameterize  
664 this process. Any foggy location on land could work but Sable Island would offer an ideal location for such a study in  
665 marine fog. It is a 43 km long, narrow (mostly < 2 km wide) sand bar in the Atlantic Ocean about 175 km offshore  
666 from Nova Scotia, Canada, and will be field site during Fatima in summer 2022. Sable Island has some vegetation,  
667 cranberry bushes and grass, wild horses and many seals and is now a National Park. Observations  
668 ([https://climate.weather.gc.ca/climate\\_normals/index\\_e.html](https://climate.weather.gc.ca/climate_normals/index_e.html)) show more than 200 (out of 720) hours of fog (visibility  
669 < 1 km) on Sable Island in the months of June and July. An upper air station (CWSA, 71600) was operated there by  
670 Environment Canada until August 2019. Taylor et al (1993) made winter storm measurements from the island as a  
671 part of the Canadian Atlantic Storms Program. The western tip of the island would be an ideal location for a tall mast  
672 or other profiling measurements with a variety of fog related and standard meteorological research instrumentation at  
673 multiple levels. Observations (-) show more than 200 (out of 720) hours of fog (visibility < 1 km) on Sable Island in  
674 the months of June and July. Taylor et al (1993) made use of Sable Island as an accessible offshore platform to study  
675 frontal passages over the sea in winter during the Canadian Atlantic Storms Program (CASP 86). Summer 2022 could  
676 be a good time to return.

677  
678

#### 679 **Code availability**

680 WRF codes used are readily available from <https://github.com/wrf-model/WRF/releases/tag/v4.2.2> . Modifications  
681 and additional details are in Cheng et al (2021a).

682

#### 683 **Author contributions**

684 ZC ,LC, PAT, YC, SA and -WW and -YC were primarily involved in aspects of the WRF code adaptation and model  
685 runs. PAT, GAI and TWB were primarily involved in reviewing background information and interpretation of the  
686 results. PAT prepared the original manuscript and its revision with contributions from all co-authors.

687

#### 688 **Competing interests**

689 The authors declare that they have no conflict of interest.

690

#### 691 **Acknowledgements**

692 Financial support for this research, for which we are very grateful, has come primarily through a Canadian NSERC  
693 Collaborative Research and Development grant program (High Resolution Modelling of Weather over the Grand  
694 Banks) with Wood Environmental and Infrastructure Solutions as the industrial partner. Initial support was also  
695 through Peter Taylor's NSERC Discovery grant. We would like to thank Anton Beljaars for providing guidance and  
696 many valuable comments as well as Ayrton Zadra and Jason Milbrandt for their help in tracking down details of  
697 Environment Canada's GEM model. Trevor VandenBoer pointed us to the aerosol work and Joe Fernando allowed  
698 two of us to attend a C-Fog meeting in 2019 where we also had useful discussions with Will Perrie and Rachel Chang.

700 **References**

- 701 Alexander, C. et al (23 co-authors): Rapid Refresh (RAP) and High Resolution Rapid Refresh (HRRR) Model  
702 Development, slides from AMS 100th Annual Meeting, available at  
703 [https://rapidrefresh.noaa.gov/pdf/Alexander\\_AMS\\_NWP\\_2020.pdf](https://rapidrefresh.noaa.gov/pdf/Alexander_AMS_NWP_2020.pdf), accessed 12 Aug 2021, 2020.
- 704 Barker, E.H.: A maritime boundary-layer model for the prediction of fog. *Boundary-Layer Meteorol* 11: 267-294,  
705 <https://doi.org/10.1007/BF02186082>, 1977.
- 706 Belair, S., Mailhot, J., Girard, C. and Vaillancourt, P.: Boundary layer and shallow cumulus clouds in a medium-range  
707 forecast of a large-scale weather system. *Mon. Wea. Rev* 133: 1938–1960, <https://doi.org/10.1175/MWR2958.1>, 2005.
- 708 Bergot, T.: Modélisation du brouillard à l'aide d'un modèle 1D forcé par des champs mésoéchelle: Application à la  
709 prévision. Ph.D. thesis, Université Paul Sabatier, Toulouse, France, 192 pp, 1993.
- 710 Bergot, T. and Guedalia, D.: Numerical forecasting of radiation fog. Part I: Numerical model and sensitivity tests.  
711 *Mon. Wea. Rev* 122: 1218–1230, [https://doi.org/10.1175/1520-0493\(1994\)122%3C1218:NFORFP%3E2.0.CO;2](https://doi.org/10.1175/1520-0493(1994)122%3C1218:NFORFP%3E2.0.CO;2),  
712 1994.
- 713 Bergot, T., Carrer, D., Noilhan, J. and Bougeault, P.: Improved site-specific numerical prediction of fog and low  
714 clouds: A feasibility study. *Weather Forecasting* 20: 627–646, <https://doi.org/10.1175/WAF873.1>, 2005.
- 715 Bergot, T., Terradellas, E., Cuxart, J., Mira, A., Liechti, O., Mueller, M. and Woetmann-Nielsen, N.: Inter comparison  
716 of Single-Column Numerical Models for the Prediction of Radiation Fog, *Journal of Applied Meteorology and*  
717 *Climatology* 46, 504-521, <https://doi.org/10.1175/JAM2475.1>, 2007.
- 718 Bott, A. and Trautmann, T.: PAFOG—A new efficient forecast model of radiation fog and low-level stratiform clouds.  
719 *Atmos. Res* 64: 191–203, [https://doi.org/10.1016/S0169-8095\(02\)00091-1](https://doi.org/10.1016/S0169-8095(02)00091-1), 2002.
- 720 Bott, A., Sievers, U. and Zdunkowski, W.: A radiation fog model with a detailed treatment of the interaction between  
721 radiative transfer and fog microphysics. *J. Atmos. Sci* 47: 2153– 2166, 1990.
- 722 Boudala, F.S., Isaac, G.A., Crawford, R. and Reid, J.: Parameterization of runway visual range as a function of  
723 visibility: Implications for numerical weather prediction models. *J. Atmos. Oceanic Technol.* 29, 177–191, 2012.
- 724 [Boutle, I. A., Finnenkoetter, A., Lock, A. P., and Wells, H.: The London Model: forecasting fog at 333m resolution, Q. J. Roy. Meteor. Soc., 142, 360–371, https://doi.org/10.1002/qj.2656, 2016.](#)
- 725 [Boutle, I., Price, J., Kudzotsa, I., Kokkola, H. and Romakkaniemi, S.: Aerosol–fog interaction and the transition to well-mixed radiation fog. Atmospheric Chemistry and Physics, 18, 11, 7827–7840, 2018.](#)
- 726 [Brown, R. and Roach, W.T.: The physics of radiation fog. II. A numerical study. Q. J. R. Meteorol. Soc 102, 335–](#)  
727 [354, 1976.](#)
- 728 [Brown, R. and Roach, W.T.: The physics of radiation fog. II. A numerical study. Q. J. R. Meteorol. Soc 102, 335–](#)  
729 [354, 1976.](#)

730 Brutsaert, W.: Evaporation into the Atmosphere: Theory, History, and Applications. Springer, Dordrecht,  
731 <http://dx.doi.org/10.1007/978-94-017-1497-6>, 1982.

732 Burkard, R., Eugster, W., Wrzesinsky, T. and Klemm, O.: Vertical divergences of fog water fluxes above a spruce  
733 forest. Atmospheric Research 64:133-145, 2002.

734 Caffrey, P.F., Ondov, J.M., Zufall, M.J. and Davidson, C.I.: Determination of size-dependent dry particle deposition  
735 velocities with multiple intrinsic elemental tracers. Environ. Sci. Technol. 32, 1615–22, 1998.

736 Charnock, H.: Wind stress on a water surface. Quart. J. Roy. Meteorol. Soc 81:639-640, 1955.

737 Chen, C., Zhang, M., Perrie, W., Chang, R., Chen, X., Duplessis, P. and Wheeler, M.: Boundary layer  
738 parameterizations to simulate fog over Atlantic Canada waters. Earth and Space Science, 7, e2019EA000703.  
739 <https://doi.org/10.1029/2019EA000703>, 2020

740 Cheng, L., Chen, Z. and Chen, Y.: ~~(2021)~~ WRF coding notes related to ~~s~~Surface deposition of marine fog,  
741 Supplementary material, <https://acp.copernicus.org/preprints/acp-2021-344/acp-2021-344-supplement.pdf>, 2021a  
742 [Cheng, L., Chen, Z., Taylor, P., Chen, Y. and Isaac, G.: Fog over Sable Island](https://bulletin.cmos.ca/fog-over-sable-island), [https://bulletin.cmos.ca/fog-over-](https://bulletin.cmos.ca/fog-over-sable-island)  
743 [sable-island](https://bulletin.cmos.ca/fog-over-sable-island), June 21, 2021b

744 de la Fuente, L., Delage, Y., Desjardines, S., MacAfee, A., Pearson, G. and Ritchie, H.: Can sea fog be inferred from  
745 operational GEM forecast fields? Pure Appl. Geophys, 164:1303–1325, 2007.

746 [Ducongé, L., Lac, C., Vié, B., Bergot, T. and Price, J.D.: Fog in heterogeneous environments: the relative importance](https://doi.org/10.1002/qj.3888)  
747 [of local and non-local processes on radiative–advective fog formation. Quart. J. of the Royal Meteorological Society,](https://doi.org/10.1002/qj.3888)  
748 [146, 2522–2546, 2020.](https://doi.org/10.1002/qj.3888)

749 ECMWF IFS Documentation CY47R1, Part IV: Physical Processes, [https://www.ecmwf.int/en/eLibrary/19748-part-](https://www.ecmwf.int/en/eLibrary/19748-part-iv-physical-processes)  
750 [iv-physical-processes](https://www.ecmwf.int/en/eLibrary/19748-part-iv-physical-processes), accessed 25 Jan 2021, 2020.

751 [Emerson, E.W., Hodshire, A.L., DeBolt, H.M., Bilsback, K.R., Pierce, J.R., McMeeking, J.R. and Farmer, D.K.:](https://doi.org/10.1073/pnas.1107260117)  
752 [Revisiting particle dry deposition and its role in radiative effect estimates. PNAS 117:26076–82, 2020.](https://doi.org/10.1073/pnas.1107260117)

753 Farmer, D.K., Boedicker, E.K. and DeBolt, H.M.: Dry Deposition of Atmospheric Aerosols: Approaches,  
754 Observations, and Mechanisms, Annu. Rev. Phys. Chem. 72:16.1–16.23, 2021.

755 Fernando, H., Gultepe, I., Dorman, C., Pardyjak, E., Wang, Q., Hoch, S., Richter, D., Creegan, E., Gabersek, S.,  
756 Bullock, T., Hocut, C., Chang, R., Alappattu, D., Dimitrova, R., Flagg, D., Grachev, A., Krishnamurthy, R., Singh,  
757 D., Lozovatsky, I., [Nagare, B. Sharma, A., Wagh, S., Wainwright, C., Wroblewski W., Yamaguchi, R., Bardoel, S.,](https://doi.org/10.1175/BAMS-D-19-0070.1)  
758 [Coppersmith, R. S., Chisholm, N., Gonzalez, E., Gunawardena, N., Hyde, O., Morrison, T., Olson, A., Perrelet, A.,](https://doi.org/10.1175/BAMS-D-19-0070.1)  
759 [Perrie, W., Wang, S. and Wauer, B. Fernand H \(2021\): C-FOG: Life of Coastal Fog. Bulletin of the American](https://doi.org/10.1175/BAMS-D-19-0070.1)  
760 [Meteorological Society](https://doi.org/10.1175/BAMS-D-19-0070.1) 102: 10.1175/BAMS-D-19-0070.1,  
761 <https://journals.ametsoc.org/view/journals/bams/102/2/BAMS-D-19-0070.1.xml>, 2021-

762 Forkel, R., Sievers, U. and Zdunkowski, W.: Fog modelling with a new treatment of the chemical equilibrium

Formatted: Font: (Default) Times New Roman, 10 pt

763 condition. *Beitr. Phys. Atmo* 60:340–360, 1987.

764 Garratt, J.R.:( *The Atmospheric Boundary layer*, Cambridge University Press, 1992.

765 Gultepe, I., Muller, M.D. and Boybeyi, Z.: A new visibility parametrization for warm fog applications in numerical  
766 weather prediction models. *J. Appl. Meteorol* 45:1469–1480, 2006.

767 Gultepe, I., Pearson, G., Milbrandt J.A., Hansen, B., Platnick, S., Taylor, P., Gordon, M., Oakley, J.P. and Cober,  
768 S.G.: The Fog Remote Sensing and Modeling (FRAM) field project. *Bull. Amer. Meteor. Soc* 90:341–359, 2009.

769 Gultepe, I., Milbrandt JA and Zhou B.: Marine Fog: A Review on Microphysics and Visibility Prediction, in *Marine*  
770 *Fog: Challenges and Advancements in Observations, Modeling and Forecasting*, D. Koraćin and C. Dorman, Eds.,  
771 Springer 345-394, 2017.

772 Hallett, J. and Christensen, L.: Splash and penetration of drops in water. *Journal de Recherches Atmospheriques*  
773 18:225–242, 1984.

774 Isaac, G.A. and Hallett, J.: Clouds and Precipitation, in *Encyclopedia of Hydrological Sciences*. Edited by M.  
775 Anderson, 2005.

776 Isaac, G.A., Bullock, T., Beale, J. and Beale, S.: Characterizing and Predicting Marine Fog Offshore Newfoundland  
777 and Labrador. *Weather and Forecasting* 35:347-365, 2020.

778 Katata, G., Nagai, H., Wrzesinsky, T., Klemm, O., Eugster, W. and Burkard, R.: Development of a land surface model  
779 including cloud water deposition on vegetation, *Journal of Applied Meteorology and Climatology*, 47, 2129-2146,  
780 2008

781 Katata, G., Kajino, M., Hiraki, T., Aikawa, M., Kobayashi, T. and Nagai, H.: A method for simple and accurate  
782 estimation of fog deposition in a mountain forest using a meteorological model. *Journal of Geophysical Research*  
783 116:D20102, 2011.

784 Katata, G.: Fogwater deposition modeling for terrestrial ecosystems: A review of developments and measurements, *J.*  
785 *Geophys. Res. Atmos* 119: 8137–8159. doi:10.1002/2014JD021669, 2014.

786 Kim, C.K. and Yum, S.S.: A numerical study of sea fog formation over cold sea surface using a one-dimensional  
787 turbulence model coupled with the Weather Research and Forecasting Model. *Boundary Layer Meteorol* 143:481–  
788 505, 2012.

789 Kim, W., Yum, S.S., Hong, J. and Song, J.I.: Improvement of Fog Simulation by the Nudging of Meteorological  
790 Tower Data in the WRF and PAFOG Coupled Model. *Atmosphere* 11: 311. doi:10.3390/atmos11030311, 2020.

791 Klemm, O., Wrzesinsky, T. and Scheer, C.: Fog water flux at a canopy top: Direct measurement versus one-  
792 dimensional model. *Atmos. Environ* 39:5375–5386, 2005.

793 Koracin, D., Dorman, C., Lewis, J., Hudson, J., Wilcox, E. and Torregrosa, A.: Marine fog: A review. *Atmospheric*  
794 *Research* 143:142–175, 2014.

795 Koraćin, D.: Modeling and forecasting marine fog. in *Marine Fog: Challenges and Advancements in Observations,*  
796 *Modeling and Forecasting*, D. Koraćin and C. Dorman, Eds., Springer, 425–475, 2017.

797 Kunkel, A.: Parameterization of droplet terminal velocity and extinction coefficient in fog models. *J. Climate Appl.*  
798 *Meteor* 23:34–41, 1984

799 Lin C, Zhang Z, Pu,Z and Wang F.: Numerical simulations of an advection fog event over Shanghai Pudong  
800 International Airport with the WRF model. *Journal of Meteorological Research* 31:874-889, 2017.

801 Lovett, G.M.: Rates and mechanisms of cloud water deposition to a subalpine balsam fir forest. *Atmos. Environ*  
802 18:361–371, 1984.

803 Maronga, B. and Bosveld, F.: Key parameters for the life cycle of nocturnal radiation fog: a comprehensive large-  
804 eddy simulation study. *Quart J R Meteorol Soc* 143:2463–2480, 2017.

805 [Mazoyer, M., Lac, C., Thouron, O., Bergot, T., Masson, V. and Musson-Genon, L.: Large eddy simulation of radiation](https://doi.org/10.1002/qj.3217)  
806 [fog: impact of dynamics on the fog life cycle, \*Atmos. Chem. Phys.\*, 17, 13017–13035, .](https://doi.org/10.1002/qj.3217)  
807 <https://acp.copernicus.org/articles/17/13017/2017/acp-17-13017-2017.pdf>, 2017.

808 Milbrandt, J.A. and Yau, M.K.: A multimoment bulk microphysics parameterization scheme. Part II: A proposed  
809 three-moment closure and scheme description. *J. Atmos. Sci* 62:3065–3081, doi:10.1175/JAS3535.1, 2005.

810 Milbrandt, J.A., Bélair, S., Faucher, M., Vallée, M., Carrera, M.L. and Glazer, A.: The Pan-Canadian high resolution  
811 (2.5 km) deterministic prediction system. *Weather and Forecasting* 31(6):1791-1816, 2016.

812 Morrison, H., Curry, J.A. and Khvorostyanov, V.I.: A new double-moment microphysics parameterization for  
813 application in cloud and climate models. Part I: description. *J Atmos Sci* 62(6):1665–1677.  
814 <https://doi.org/10.1175/JAS3446.1>, 2005.

815 Morrison, H. and Milbrandt, J.A.: Parameterization of ice microphysics based on the prediction of bulk particle  
816 properties. Part I: Scheme description and idealized tests. *J. Atmos. Sci* 72:287–311, [https://doi.org/10.1175/JAS-D-](https://doi.org/10.1175/JAS-D-14-0065.1)  
817 [14-0065.1](https://doi.org/10.1175/JAS-D-14-0065.1), 2015.

818 Musson-Genon, L.: Numerical simulation of a fog event with a one-dimensional boundary-layer model. *Mon. Weather*  
819 *Rev* 115:29-39, 1987.

820 Olson, J.B., Kenyon JS, Angevine WA, Brown JM, Pagowski M. and Suselj, K.: A Description of the MYNN-EDMF  
821 Scheme and the Coupling to Other Components in WRF–ARW. NOAA Technical Memorandum OAR GSD-61.  
822 <https://doi.org/10.25923/n9wm-be49>, 2019.

823 Pinnick, R., Hoihjelle, D.L., Fernandez, G., Stenmark, E.B., Lindberg, J.D., Hoidale, G.B. and Jennings, S.G.:  
824 Vertical structure in atmospheric fog and haze and its effect on visible and infrared extinction. *J. Atmos. Sci* 35:2020–  
825 2032, 1978.

826 [Price, J.D., Lane, S., Boutle, I.A., Smith, D.K.E., Bergot, T., Lac, C., Duconge, L., McGregor, J., Kerr-Munslow, A.,](https://doi.org/10.1002/qj.3217)  
827 [Pickering, M. and Clark, R.: LANFEX: a field and modeling study to improve our understanding and forecasting of](https://doi.org/10.1002/qj.3217)

828 [radiation fog. Bulletin of the American Meteorological Society, 99, 2061–2077, 2018](#)

829 Qi, J., Yu, Y., Yao, X., Gang, Y. and Gao, H.: Dry deposition fluxes of inorganic nitrogen and phosphorus in  
830 atmospheric aerosols over the Marginal Seas and Northwest Pacific. *Atmos. Res.* 245:105076, 2020.

831 Richter, D.H., MacMillan, T. and Wainwright, C.: A Lagrangian Cloud Model for the Study of Marine Fog. *Boundary-*  
832 *Layer Meteorol.*, <https://doi.org/10.1007/s10546-020-00595-w>, 2021.

833 Rogers, R.R. and Yau, M.K.: *A short course in Cloud Physics*, Pergamon, Oxford, 1989.

834 Schemenauer, R.S. and Cereceda, P.: Fog-Water Collection in Arid Coastal Locations. *Ambio* 20(7):303–308, 1991.

835 Sehmel, G. and Sutter, S.: Particle deposition rates on a water surface as a function of particle diameter and air velocity.  
836 Rep. BNWL-1850, Battelle Pac. Northwest Labs, Richland, WA, 1974.

837 Schwenkel, J. and Maronga, B.: Large-eddy simulation of radiation fog with comprehensive two-moment bulk  
838 microphysics: impact of different aerosol activation and condensation parameterizations, *Atmos. Chem. Phys*  
839 19:7165–7181, <https://doi.org/10.5194/acp-19-7165-2019>, 2019

840 Schwenkel, J., and Maronga, B.: Towards a better representation of fog microphysics in large-eddy simulations based  
841 on an embedded Lagrangian cloud model, *Atmosphere* 11:466. <https://doi.org/10.3390/ATMOS11050466>, 2020.

842 Shuttleworth, W.J.: The exchange of wind-driven fog and mist between vegetation and the atmosphere. *Boundary-*  
843 *Layer Meteorol* 12:463-489, 1977.

844 Siebert, J., Bott, A., and Zdunkowski, W.: Influence of a vegetation-soil model on the simulation of radiation fog.  
845 *Beitr. Phys. Atmos* 65:93–106., 1992a.

846 Siebert, J., Sievers, U., and Zdunkowski, W.: A one-dimensional simulation of the interaction between land surface  
847 processes and the atmosphere. *Boundary-Layer Meteorol* 59:1–34, 1992b.

848 Skamarock, W.C., Klemp, J.B., Dudhia, J., Gill, D.O., Liu, Z., Berner, J., Wang, W., Powers, J.G., Duda, M.G.,  
849 Barker, D.M. and Huang, X-Y.: A Description of the Advanced Research WRF Model Version 4.3,  
850 <http://dx.doi.org/10.5065/1dfh-6p97>, 2021

851 [Smith, D.K., Renfrew, I.A., Dorling, S.R., Price, J.D. and Boutle, I.A.: Sub-km scale numerical weather prediction](#)  
852 [model simulations of radiation fog. Q J R Meteorol Soc., 147, 746–763, https://doi.org/10.1002/qj.3943, 2021](#)

853 Stolaki, S., Pytharoulis, I. and Karacostas, T.: A study of fog characteristics using a coupled WRF-COBEL model over  
854 Thessaloniki Airport, Greece. *Pure and Applied Geophysics* 169:961-981, 2012.

855 Taylor, G.I.: The formation of fog and mist. *Quart. J. Roy. Meteor. Soc* 43:241–268, [https://doi.org/10.1002/](https://doi.org/10.1002/qj.49704318302)  
856 [qj.49704318302](https://doi.org/10.1002/qj.49704318302), 1917.

857 [Taylor, P.A.: Constant Flux Layers with Gravitational Settling: with links to aerosols, fog and deposition velocities](#)  
858 [over water, ACP discussion paper.: https://acp.copernicus.org/preprints/acp-2021-594/, 2021](#)

859 Taylor, P.A., Salmon, J.R. and Stewart, R.E.: Mesoscale observations of surface fronts and low pressure centres in

860 Canadian East Coast winter storms. *Boundary-Layer Meteorol*, 64, 15–54, <https://doi.org/10.1007/BF00705661>,  
861 1993

862 Teixeira, J.: Simulation of fog with the ECMWF prognostic cloud scheme. *Quarterly Journal of the Royal*  
863 *Meteorological Society*,125(554):529-552, 1999.

864 Tiedtke, M.: Representation of clouds in large-scale models. *Mon. Weather Rev* 121:3040-3061, 1993.

865 Wainwright, C. and Richter, D.: Investigating the Sensitivity of Marine Fog to Physical and Microphysical Processes  
866 Using Large-Eddy Simulation. *Boundary-Layer Meteorol*. <https://doi.org/10.1007/s10546-020-00599-6>, 2021

867 Williams, R. M.: A model for the dry deposition of particles to natural water surfaces, *Atmos. Environ.* 16, 1933-  
868 1938, 1982.

869 Wilkinson, J.M., Porson, A.N.F., Bornemann, F.J., Weeks, M., Field, P.R. and Lock, A.P.: Improved microphysical  
870 parametrization of drizzle and fog for operational forecasting using the Met Office Unified Model. *Quart. J. Roy.*  
871 *Meteor. Soc* 139:488–500, <https://doi.org/10.1002/qj.1975>, 2013

872 WMO: Variable: Meteorological Optical Range (MOR) (surface) accessed 4 Jan 2021, [https://www.wmo-](https://www.wmo-sat.info/oscar/variables/view/meteorological_optical_range_mor_surface)  
873 [sat.info/oscar/variables/view/meteorological\\_optical\\_range\\_mor\\_surface](https://www.wmo-sat.info/oscar/variables/view/meteorological_optical_range_mor_surface), 2020.

874 Yang, D., Ritchie, H., Desjardins, S., Pearson, G., MacAfee, A. and Gultepe, I.: High-Resolution GEM-LAM  
875 Application in Marine Fog Prediction: Evaluation and Diagnosis, *Weather and Forecasting* 25:727–748, 2010.

876 Yang, Y., Gao, S.: The impact of turbulent diffusion driven by fog-top cooling on sea fog development. *Journal of*  
877 *Geophysical Research: Atmospheres*,125:e2019JD031562. <https://doi.org/10.1029/2019JD031562>, 2020.

878 Zdunkowski, W.G. and Barr, A.E.: A Radiative-Conductive Model for the Prediction of Radiation Fog, *Boundary-*  
879 *Layer Meteorol* 3:152-177 , 1972.

880 [Zhang, X., Musson-Genon, L., Dupont, E., Milliez, M., and Carissimo, B.: On the Influence of a Simple Microphysics](#)  
881 [Parametrization on Radiation Fog Modelling: A Case Study During ParisFog. \*Bound.-Lay. Meteorol.\*, 151, 293–315,](#)  
882 [2014.](#)

883 Zhou, B. and Du, J.: Fog Prediction from a Multimodel Mesoscale Ensemble Prediction System, *Weather and*  
884 *Forecasting* 25(1):303–322. <https://doi.org/10.1175/2009WAF2222289.1>, 2010.

885 Zufall, M.J., Davidson, C.I., Caffrey, P.F. and Ondov, J.M.: Airborne concentrations and dry deposition fluxes of  
886 particulate species to surrogate surfaces deployed in southern Lake Michigan. *Environ. Sci. Technol.* 32:1623–28,  
887 1998.

888 -----